Crystal structure of the DNA nucleotide excision repair enzyme UvrB from *Thermus thermophilus*

Mischa Machius, Lisa Henry, Maya Palnitkar, and Johann Deisenhofer*

Howard Hughes Medical Institute and Department of Biochemistry, University of Texas Southwestern Medical Center at Dallas, 5323 Harry Hines Boulevard, Dallas, TX 75235-9050

Contributed by Johann Deisenhofer, August 16, 1999

Nucleotide excision repair (NER) is the most important DNA-repair mechanism in living organisms. In prokaryotes, three enzymes forming the UvrABC system initiate NER of a variety of structurally different DNA lesions. UvrB, the central component of this system, is responsible for the ultimate DNA damage recognition and participates in the incision of the damaged DNA strand. The crystal structure of *Thermus thermophilus* UvrB reveals a core that is structurally similar to core regions found in helicases, where they constitute molecular motors. Additional domains implicated in binding to DNA and various components of the NER system are attached to this central core. The architecture and distribution of DNA binding sites suggest a possible model for the DNA damage recognition process.

Nucleotide excision repair (NER) is a universal DNA repair mechanism by which virtually any DNA damage can be removed through incisions on both sides of the lesion (1–4). Damages recognized by this system are chemically and structurally diverse and include bulky adducts, such as intercalators like psoralen or the benzo[a]pyrene-guanine adduct, as well as smaller lesions that induce minor helical distortions, such as apurinic/apyrimidinic sites or O^6-methyl-guanine. NER furthermore serves as a proof-reading mechanism during transcription (5, 6). In humans, the NER system is an important defense mechanism against two major carcinogens, sunlight and cigarette smoke. Defects in NER cause several diseases that are associated with increased incidences of cancer, most notably xeroderma pigmentosum (7, 8).

NER is a complicated reaction cascade that can be divided into three steps, DNA damage recognition, dual incision, and repair synthesis and ligation (1, 3, 4, 9, 10). In humans, nucleotide excision requires the combined action of at least 16 polypeptides (11). By contrast, prokaryotes require only three enzymes, UvrA, UvrB, and UvrC, collectively called the UvrABC system. Because of the relative simplicity, the UvrABC system has been studied extensively, particularly in *Escherichia coli*, and serves as a model system for NER (1, 3, 4, 9, 10). Initial damage recognition is accomplished by UvrA, which forms a $UvrA_2B$ complex with UvrB and probes DNA for lesions (12). The characteristics of the interactions between DNA lesions and the $UvrA_2B$ particle suggest a multilevel recognition process in which the lesion seems to be recognized not by its chemical nature but, rather, by its effect on the flexibility of DNA (1, 3, 4, 9, 10). Once a damaged site is detected, UvrA and UvrB work together in an ATP-dependent reaction to form a specific and stable complex between UvrB and the damaged DNA (12–15), a process referred to as the ultimate damage recognition (16) or High Resolution Recognition (17). In the resulting preincision complex, the DNA is sharply bent and locally denatured (18–21). The endonuclease UvrC subsequently recognizes the preincision complex and, together with UvrB, nicks the damaged strand 3′ and 5′ of the lesion (22–24). The resulting 12- to 13-nt-long fragment is ultimately removed by UvrD (helicase II), and the gap is filled by DNA polymerase and ligase.

As is apparent from the brief summary given above, UvrB, a 76-kDa multifunctional protein, is the central component in the NER reaction cascade (1, 3, 4, 9, 10, 16, 25). UvrB interacts first with UvrA, then with UvrC, and finally with helicases and polymerases that complete excision repair. Furthermore, it is a damage-specific DNA-binding protein with helicase and strand-separating activities, which are ATP-driven functionalities that are latent and become active only on complex formation with UvrA (26–29). Here we present the crystal structure of *Thermus thermophilus* UvrB (Tt UvrB), providing the first structural information on a component of a nucleotide excision repair system.

Methods

Data Collection and Structure Determination. Full-length Tt UvrB (30) was expressed in *E. coli* and was crystallized as described by Shibata *et al.* (31). Tt UvrB crystallizes with the symmetry of space group $P3_221$ with cell dimensions $a = b = 135.4$ Å, $c = 106.5$ Å, and one molecule in the asymmetric unit. The crystal structure was determined by single isomorphous replacement/anomalous scattering from a xenon derivative. The xenon derivative was prepared by pressurizing a Tt UvrB crystal with 500 psi of xenon gas for 15 min at room temperature (xenon chamber kindly provided by Z. Wang, University of Texas Southwestern Medical Center at Dallas). The chamber then was depressurized within 15 seconds and the crystal flash-frozen in liquid propane within another 5 seconds. Diffraction data from a native crystal to 1.83-Å Bragg spacing and from a xenon-derivatized crystal to 1.9-Å Bragg spacing were collected at the Stanford Synchrotron Radiation Laboratory (Stanford, CA) beamline 9-1. The data were reduced with the program package DENZO/SCALEPACK (32). Bijvoet pairs were kept separate for the xenon derivative. Xenon sites were identified and refined to 3.0 Å with CNS 0.5 (33), resulting in a figure of merit of 0.38. The phases were further improved by density modification (CNS 0.5), including histogram matching, solvent flipping, and phase extension to 2.0 Å, resulting in a final figure of merit of 0.83 (Fig. 1). Data collection and single isomorphous replacement/anomalous scattering phasing statistics are shown in Table 1.

Model Building and Structure Refinement. Model building was done with the program O (34). Structure refinement was carried out with the program CNS 0.5, using cycles of simulated annealing, conjugate gradient minimization, and calculation of individual temperature factors. Calculation of overall aniso-

Abbreviations: Ec UvrB, *Escherichia coli* UvrB; Tt UvrB, *Thermus thermophilus* UvrB; NER, nucleotide excision repair.

Data deposition: The structural coordinate has been deposited in the Protein Data Bank, www.rcsb.org (PDB ID code 1c4o).

*To whom reprint requests should be addressed. E-mail: Johann.Deisenhofer@email.swmed.edu.

The publication costs of this article were defrayed in part by page charge payment. This article must therefore be hereby marked "*advertisement*" in accordance with 18 U.S.C. §1734 solely to indicate this fact.

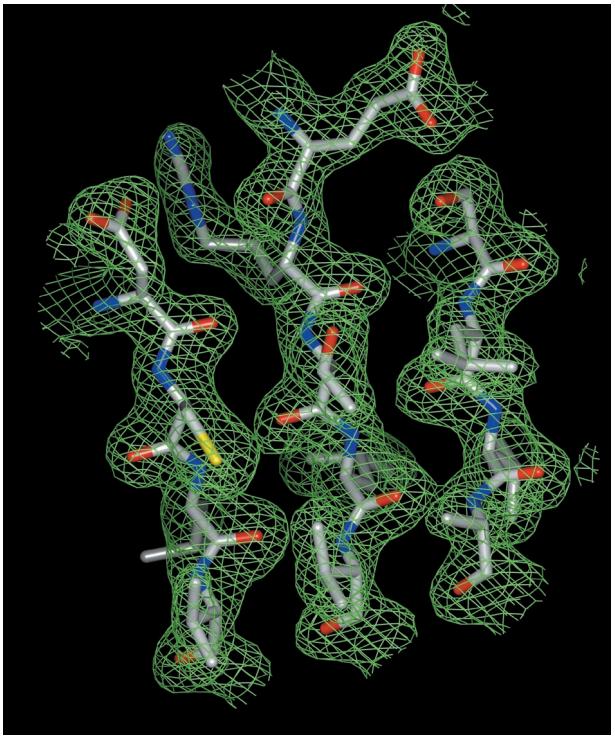

Fig. 1. Single isomorphous replacement/anomalous scattering electron density (green) contoured at 2.0 σ after density modification with the final model superimposed. Shown is the core of helicase domain H2. Carbon atoms are in gray, oxygen atoms in red, nitrogen atoms in blue, and sulfur atoms in yellow.

tropic temperature factors and bulk solvent correction were used throughout. Water molecules were added where stereochemically reasonable after the protein part was completed. During model building, it became clear that large portions of the Tt UvrB structure are disordered. The disordered regions exhibit electron density that is unconnected and could not be traced. Side chains with poorly defined density were truncated to alanine for refinement purposes. The final model contains residues 2–157, residues 236–583, a 10-residue peptide whose sequence could not be unequivocally assigned, four sulfate ions, two molecules of the detergent β-octyl glucoside, and 270 water molecules. The N-terminal methionine is removed during expression (30). Residues 158–235 and 584–665 are disordered in the crystal structure and could not be traced in the electron density. The R_{free} value is 25.9%, and the R_{work} value is 24.0% (Table 2). Given the presence of rather large disordered regions, our Tt UvrB crystals diffracted x-rays exceptionally well, and the refined structure of the core has low R_{work} and R_{free} values, indicating that the disordered regions can efficiently be modeled as bulk solvent.

Table 1. Data collection and structure determination

		Native	Xenon*
Data collection			
Wavelength, Å		1.08	1.08
Resolution, Å		1.83	1.90
Completeness	overall, %	98.8	93.5
	last shell, %	91.2	95.9
R_{sym}†	overall, %	5.2	5.2
	last shell, %	80.6	74.1
I/σ	overall	28.6	23.0
	last shell	1.8	1.8
Multiplicity	overall	5.9	3.9
	last shell	4.6	3.3
SIRAS			
Number of sites		–	4
Resolution, Å		–	3.0
R_{Cullis}‡		–	0.72
Phasing power‡		–	1.06
Figure of merit		–	0.38

SIRAS, single isomorphous replacement/anomalous scattering.
*Bijvoet pairs were kept separate.
†$R_{sym} = 100(\Sigma_h|I_h - \langle I\rangle|)/(\Sigma_h I_h)$, where $\langle I\rangle$ is the mean intensity of all symmetry-related reflections I_h.
‡$R_{Cullis} = (\Sigma|F_{PH} \pm F_P| - F_{H(calc)})/(\Sigma|F_{PH} \pm F_P|)$ for centric reflections; phasing power $= [\Sigma F_{H(calc)}^2/\Sigma F_{PH(obs)} - F_{PH(obs)}^2]^{1/2}$.

Table 2. Structure refinement

Data		
Resolution range, Å		28.4-1.90
Reflections	Workingset	160,479
	Freeset	3,189
Completeness, %		92.3
σ-cutoff		0.0
Atoms in model		
Protein (nonhydrogen)		3,928
β-octylglucoside		40
Sulfate		20
Water		270
Refinement parameters		
R_{work}*, %		24.0
R_{free}*, %		25.9
Average atomic B factors, Å^2		
Protein		35.9
β-octylglucoside		52.9
Sulfate		65.9
Water		41.6
Deviation from ideality, rms deviation		
Bonds, Å		0.013
Angles, °		1.504
Dihedrals, °		23.047
Inpropers, °		1.019

*$R = 100(\Sigma|F_{obs} - F_{calc}|)/(\Sigma F_{obs})$, where F_{obs} and F_{calc} are observed and calculated structure factors, respectively.

Results and Discussion

Overall Structure. Our crystal structure of Tt UvrB shows three domains (referred to as domains H1, H2, and P1) (Fig. 2*A*). Domains H1 and H2, which are connected by a linker, both contain a large central β-sheet flanked by several α-helices. They are structurally very similar but unrelated in sequence. Domain H2 is composed of a contiguous polypeptide chain (residues 409–583). Protrusions emerging from loop regions in domain H1 make up the peripheral domain P1. This domain contains three ''arms'' (A1, A2, and A3) that surround a hole lined mainly with aromatic residues (Fig. 3). Arm A1 is composed of a hairpin structure whereas A2 and A3 each encompass two helices connected by a turn. A3 also contains a loop region at its base that contributes to the wall surrounding the hole. The side chains of Y89 and E302 form a bridge that spans the hole between arms A1 and A2. The two regions that are disordered in our crystal structure are referred to as region P2 (residues 158–235), located between domain H1 and arm A2, as well as region C (residues 584 to 665) at the C terminus of UvrB (Figs. 2*A* and 4). Our domain nomenclature is based on the three-dimensional structure of Tt UvrB and deviates from the scheme used in ref. 35, which is based on limited proteolysis experiments.

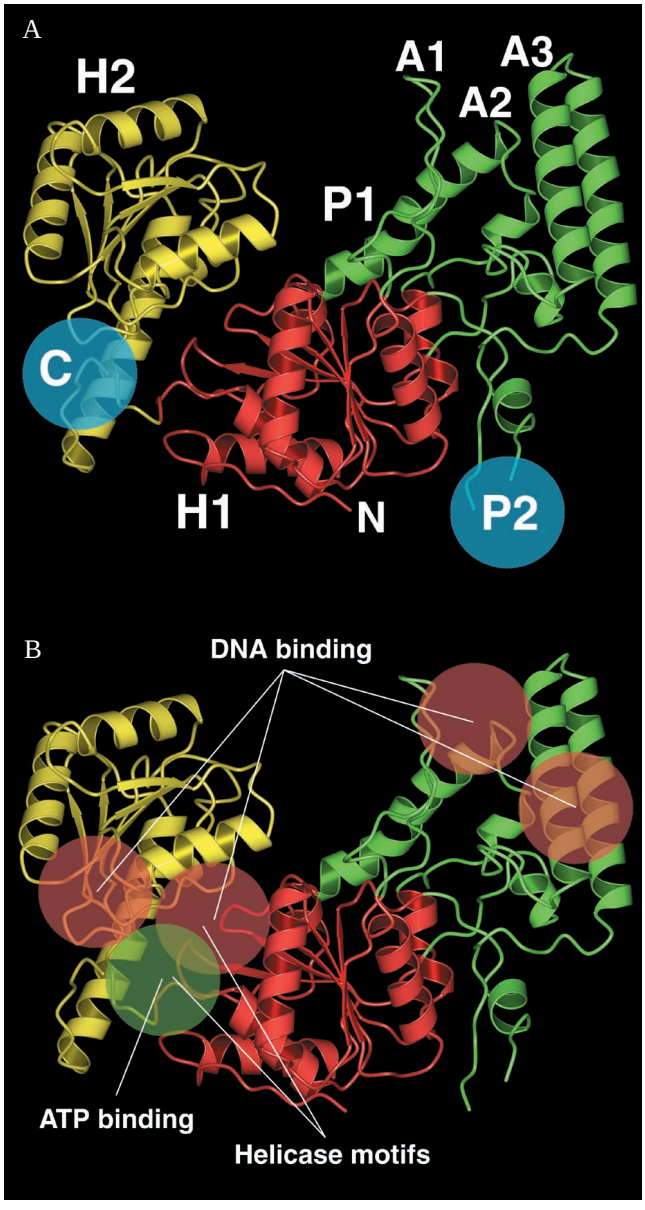

Fig. 2. (*A*) Overall topology of Tt UvrB. Domains not visible in the electron density are indicated by blue circles. (*B*) Functional sites in UvrB. Figs. 1, 2, and 3 were made with BOBSCRIPT (53), GRASP (54), POV-RAY (Persistence of Vision Raytracer, v3.02, POV-Team, www.povray.org), and GL_RENDER (L. Esser, University of Texas Southwestern Medical Center at Dallas).

Structural Similarity to Helicases. Domains H1 and H2 of UvrB form a core, which is structurally similar to the core regions of RNA and DNA helicases as represented by the known three-dimensional structures for hepatitis C RNA helicase (HCV) (36), *Bacillus stearothermophilus* DNA helicase (PcrA) (37), and *E. coli* Rep helicase (38). In helicases, these two domains constitute a molecular motor that couples the energy derived from ATP hydrolysis to the mechanical action of DNA or RNA unwinding. The presence of such helicase domains in UvrB had been suspected (35) because UvrB has helicase activity and because sequence comparisons have revealed typical helicase consensus motifs (39). The helicase motifs decorate the bottom and sides of the cleft between helicase domains H1 and H2 (Figs. 2*B* and 4).

Mutagenesis studies, epitope mapping, and limited proteolysis experiments have revealed the regions responsible for the different functionalities in UvrB (25, 35, 40, 41), and many residues have been assigned specific roles. Although most of these studies were carried out with *E. coli* UvrB (Ec UvrB), the sequence similarity to Tt UvrB is sufficiently high [55% identity, 70% similarity (Fig. 4)] to allow interpretation of the effects observed in the *E. coli* enzyme in the light of the Tt UvrB structure.

ATP Binding Site. The ATP binding site inferred from the presence of Walker A and B motifs (identical to helicase motifs I and II) in UvrB is located at the bottom of the cleft between helicase domains H1 and H2 (Fig. 2*B*). We were unable to observe directly the binding of adenine nucleotides to the Walker ATP binding motif in Tt UvrB, although we assured the ability of our purified Tt UvrB to bind adenine nucleotides by measuring enhanced fluorescence emission of the ADP and ATP analogs TNP-ADP and TNP-ATP [TNP = 2′(3′)-*O*-(2, 4, 6-trinitrophenyl)] on addition of Tt UvrB (42) (data not shown). The absence of ADP or ATP in our Tt UvrB crystals is probably attributable to the fact that crystal contacts force the helicase domains into a relative orientation that precludes nucleotide binding. In helicases, a large range of angles between the central helicase domains has been observed, indicating that the linker region is flexible (38, 43–45). Because residues belonging to both helicase domains are required for ATP binding, it is likely that only certain relative orientations of the domains are compatible with a fully functional nucleotide binding site.

DNA Binding. Several regions in UvrB bind to DNA (25, 46–48). The initial contacts between UvrB and DNA are nonspecific and mediated mainly by electrostatic interactions with the DNA backbone (46). Mutation of residues G509, R540, and R544, implicated in the nonspecific interaction between DNA and Ec UvrB, results in modulated DNA binding, which, in turn, leads to reduced ATPase activity (49). The mutants do not exhibit helicase activity and fail to form the preincision complex. Residues 509, 540, and 544 belong to the helicase motifs V and VI located in the cleft between the helicase domains. This region is lined with a number of positively charged residues, a structural feature that is shared with HCV, PcrA, and Rep. For these helicases, it was shown that residues located in this region are involved in DNA binding (helicase motifs I, III, and V) or in the allosteric transduction of DNA binding effects to the ATP binding site at the bottom of the cleft (helicase motif VI) (38, 50, 51). It is therefore likely that UvrB features a similar mode of interaction with DNA.

After the nonspecific interaction with DNA, unwinding and strand separation carried out by the $UvrA_2B$ complex expose the bases in the DNA and lead to the formation of specific interactions with UvrB. In Ec UvrB, residues E99, E266, F366, F497, E514, and E640 have been implicated in such interactions (25, 46–48). The equivalent residues in Tt UvrB map topologically to four different regions (Fig. 2*B*): E96 (equivalent to E99 in Ec UvrB), in arm A1, and F361 (equivalent to F366 in Ec UvrB), in arm A3, are located close to the hole in domain P1 (Fig. 3*B*); E261 (equivalent to E266 in Ec UvrB) is located in the first helix of arm A3 in domain P1; Y491 (equivalent to F497 in Ec UvrB) and E508 (equivalent to E514 in Ec UvrB) are located in domain H2 in loop regions at the N-terminal side of the central β-sheet; and E618 (equivalent to E640 in Ec UvrB) belongs to the C-terminal part of UvrB, which is disordered in our crystal structure. Most of these residues are solvent-accessible and can therefore interact directly with DNA. In particular, it has been shown that F366 in Ec UvrB makes direct contacts to thymine dimers in damaged single-stranded DNA (25). Unexpectedly, however,

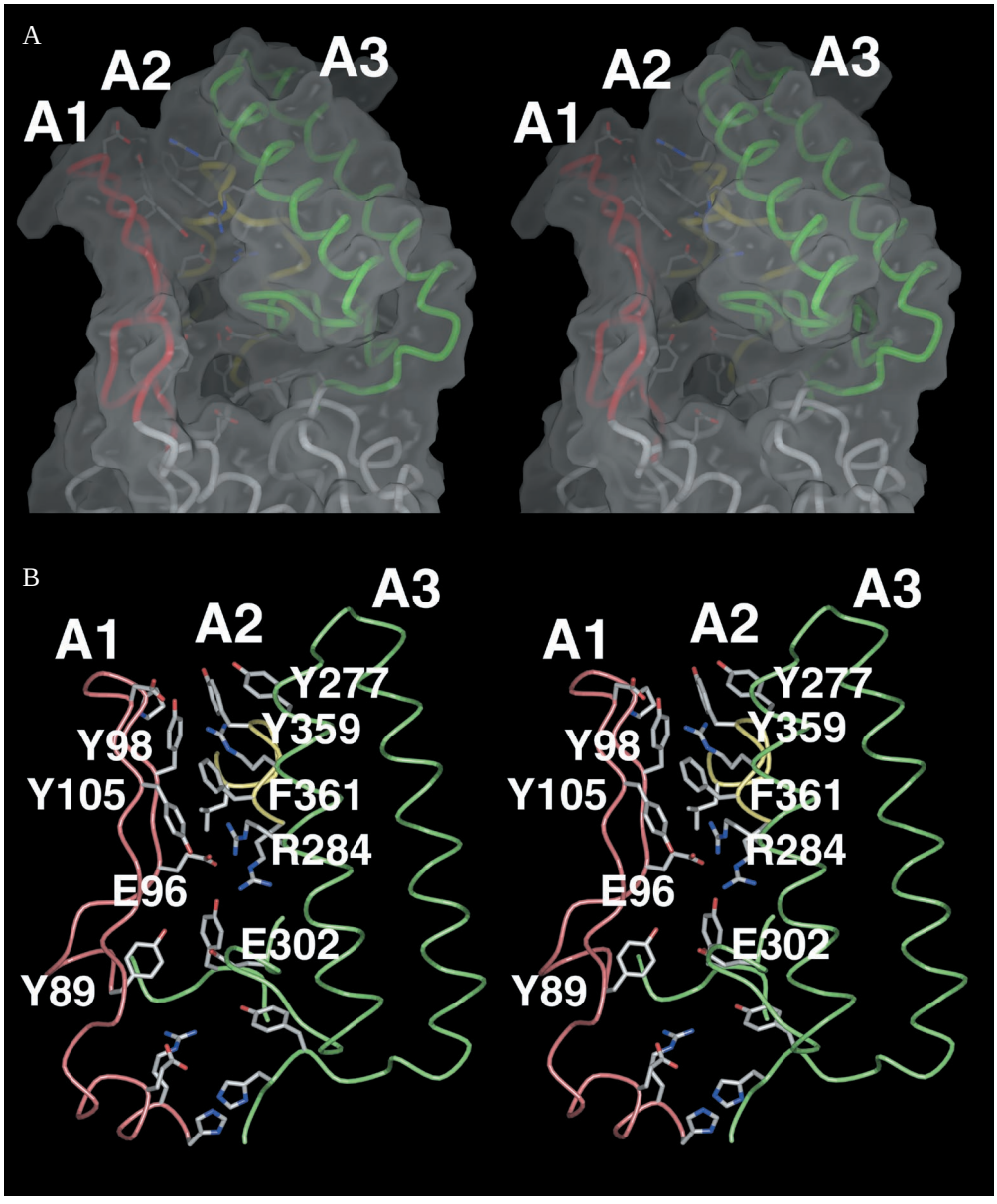

Fig. 3. (*A*) Stereoview of the surface of the hole in domain P1 with underlying residues. Arm A1 is in red, A2 is in green, and A3 is in yellow. (*B*) Stereoview showing the interactions in the roof region above the hole. These interactions involve E96 and F361, which are implicated in DNA binding.

E96 and F361 in Tt UvrB are strongly involved in interactions within UvrB. E96 establishes an ionic interaction with R284, and F361 participates in a complex network of aromatic stacking interactions with Y98, F105, and Y359 (Fig. 3*B*). These interactions stabilize the roof above the hole in domain P1 in which the three arms A1, A2, and A3 come into contact (Fig. 3). The basal part of arm A1, which surrounds the hole, appears to be quite flexible, as indicated by weak electron density and by temperature factors that are 15–20 $Å^2$ higher than those in the opposing arms. For E96 and F361 to bind to DNA lesions, the specific interactions within UvrB must be exchanged for interactions with the damaged DNA. This is possible only if binding of DNA and/or UvrA causes arm A1 to move outwards relative to the opposing arms.

The structural elements responsible for the interactions of UvrB with UvrA and UvrC have been mapped to areas that we have identified as regions P2 and C (25, 35, 40, 41) (Figs. 2*A* and 4). These two regions are largely disordered in our Tt UvrB crystal structure. They either do not have defined structures until they are involved in binding UvrA and/or UvrC and/or DNA, or they do have defined structures but exhibit varying orientations with respect to the rest of the molecule.

Mechanism of DNA Damage Recognition. The most enigmatic features of the UvrABC system are how it discriminates between substrate and nonsubstrate DNA structures and how it recognizes a wide array of different DNA lesions. The structural data described here may shed some light onto the ultimate damage recognition process carried out by UvrB. Interactions with UvrA and DNA lead to conformational changes that might ultimately expose residues in the interface between arm A1 and arms A2 and A3 so that specific interactions with the damaged DNA can be formed. This process, which is based on the flexibility and possible movements of arm A1, potentially traps the damaged DNA strand and fixes the DNA lesion at a well defined location in UvrB.

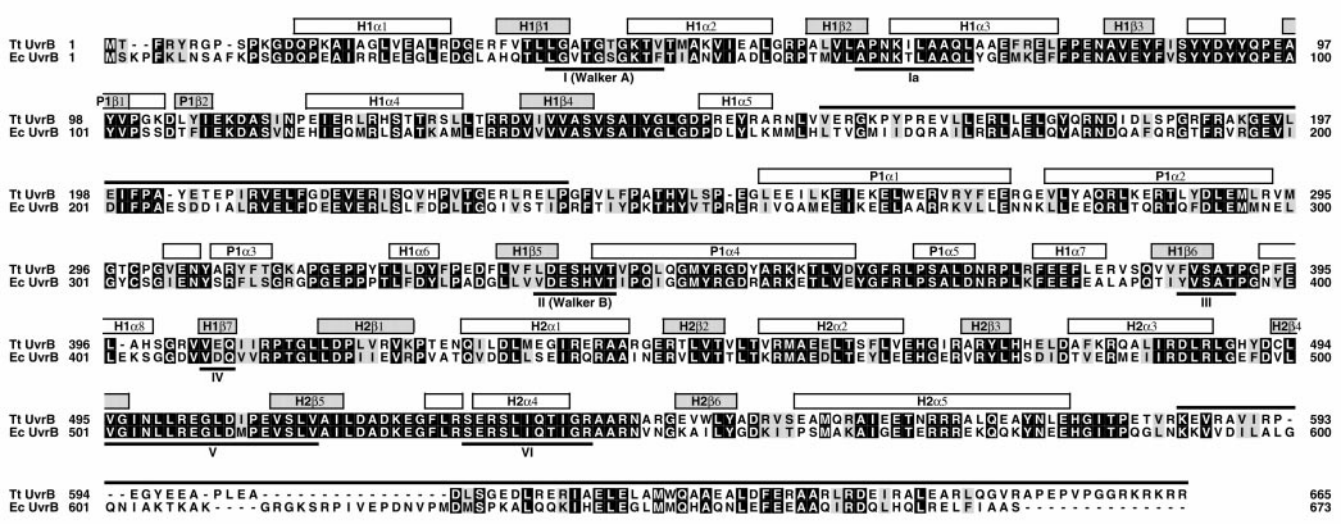

Fig. 4. Sequence alignment of Tt and Ec UvrB (30). Conserved residues are indicated by a black background. Similar residues (R/K, D/E, S/T, L/I/V/F/Y/M) have a gray background. Secondary structure elements are indicated above the sequences (α-helices are represented by white boxes, β-strands by gray boxes) and are numbered sequentially (first two letters denote the corresponding domain). The regions that are disordered in the crystal structure are marked by a black line above the sequences. Helicase consensus sequences (39) are labeled with Roman numbers.

Subsequent binding of UvrC then could establish a complex in which the DNA is aligned with appropriate catalytic sites where the incisions in the damaged strand occur. This model would explain why the incisions are located at precisely three to five phosphodiester bonds 3′ of the lesion and eight phosphodiester bonds 5′ of the lesion (52). Furthermore, the flexibility of arm A1 would allow modulation of the size of the trap so that different kinds of lesions can be accommodated. This feature might explain the ability of UvrB to process a wide variety of structurally unrelated DNA lesions.

The authors thank Chung-I Chang for help in the early stages of the project, Zhenming Wang for providing the xenon-derivatization chamber, and Gabrielle Rudenko, Chad Brautigam, Aziz Sancar, Lawrence Grossman, and Kirsten Fischer Lindahl for helpful discussions and critical reading of the manuscript.

1. Van Houten, B. & Snowden, A. (1993) *BioEssays* **15,** 51–59.
2. Friedberg, E. C., Bonura, T., Love, J. D., McMillan, S., Radany, E. H. & Schultz, R. A. (1981) *J. Supramol. Struct. Cell. Biochem.* **16,** 91–103.
3. Sancar, A. (1996) *Annu. Rev. Biochem.* **65,** 43–81.
4. Grossman, L., Lin, C.-L. & Ahn, Y. (1998) in *DNA Damage and Repair*, ed. Nickoloff, J. A. & Hoekstra, M. F. (Humana, Totowa, NJ), Vol. 1.
5. Bohr, V. A., Smith, C. A., Okumoto, D. S. & Hanawalt, P. C. (1985) *Cell* **40,** 359–369.
6. Mellon, I. & Hanawalt, P. C. (1989) *Nature (London)* **342,** 95–98.
7. Cleaver, J. E. (1968) *Nature (London)* **218,** 652–656.
8. Cleaver J. E. & Kraemer, K. H. (1989) in *The Metabolic Basis of Inherited Disease*, eds. Scriver, C. R., Beaudet, A. L., Sly, W. S. & Valle, D. (McGraw–Hill, New York), Vol. 2.
9. Friedberg, E. C. (1996) *Annu. Rev. Biochem.* **65,** 15–42.
10. Lehmann, A. R. (1995) *Trends Biochem. Sci.* **20,** 402–405.
11. Mu, D., Park, C. H., Matsunaga, T., Hsu, D. S., Reardon, J. T. & Sancar, A. (1995) *J. Biol. Chem.* **270,** 2415–2418.
12. Orren, D. K. & Sancar, A. (1989) *Proc. Natl. Acad. Sci. USA* **86,** 5237–5241.
13. Orren, D. K., Selby, C. P., Hearst, J. E. & Sancar, A. (1992) *J. Biol. Chem.* **267,** 780–788.
14. Visse, R., de Ruijter, M., Moolenaar, G. F. & van de Putte, P. (1992) *J. Biol. Chem.* **267,** 6736–6742.
15. Delagoutte, E., Bertrand-Burggraf, E., Dunand, J. & Fuchs, R. P. (1997) *J. Mol. Biol.* **266,** 703–710.
16. Lin, J. J. & Sancar, A. (1992) *Mol. Microbiol.* **6,** 2219–2224.
17. Gordienko, I. & Rupp, W. D. (1997) *EMBO J.* **16,** 880–888.
18. Oh, E. Y. & Grossman, L. (1987) *Proc. Natl. Acad. Sci. USA* **84,** 3638–3642.
19. Shi, Q., Thresher, R., Sancar, A. & Griffith, J. (1992) *J. Mol. Biol.* **226,** 425–432.
20. Visse, R., King, A., Moolenaar, G. F., Goosen, N. & van de Putte, P. (1994) *Biochemistry* **33,** 9881–9888.
21. Gordienko, I. & Rupp, W. D. (1997) *EMBO J.* **16,** 889–895.
22. Lin, J. J. & Sancar, A. (1990) *J. Biol. Chem.* **265,** 21337–21341.
23. Moolenaar, G. F., Bazuine, M., van Knippenberg, I. C., Visse, R. & Goosen, N. (1998) *J. Biol. Chem.* **273,** 34896–34903.
24. Zou, Y., Walker, R., Bassett, H., Geacintov, N. E. & Van Houten, B. (1997) *J. Biol. Chem.* **272,** 4820–4827.
25. Hsu, D. S., Kim, S. T., Sun, Q. & Sancar, A. (1995) *J. Biol. Chem.* **270,** 8319–8327.
26. Hildebrand, E. L. & Grossman, L. (1998) *J. Biol. Chem.* **273,** 7818–7827.
27. Thiagalingam, S. & Grossman, L. (1993) *J. Biol. Chem.* **268,** 18382–18329.
28. Orren, D. K. & Sancar, A. (1990) *J. Biol. Chem.* **265,** 15796–15803.
29. Oh, E. Y., Claassen, L., Thiagalingam, S., Mazur, S. & Grossman, L. (1989) *Nucleic Acids Res.* **17,** 4145–4159.
30. Kato, R., Yamamoto, N., Kito, K. & Kuramitsu, S. (1996) *J. Biol. Chem.* **271,** 9612–9618.
31. Shibata, A., Nakagawa, N., Sugahara, M., Masui, R., Kato, R., Kuramitsu, S. & Fukuyama, K. (1999) *Acta Crystallogr. D* **55,** 704–705.
32. Otwinowski, Z. & Minor, W. (1997) *Methods Enzymol.* **276,** 307–326.
33. Brunger, A. T., Adams, P. D., Clore, G. M., DeLano, W. L., Gros, P., Grosse-Kunstleve, R. W., Jiang, J. S., Kuszewski, J., Nilges, M., Pannu, N. S., *et al.* (1998) *Acta Crystallogr. D* **54,** 905–921.
34. Jones, T. A., Zou, J. Y., Cowan, S. W. & Kjeldgaard (1991) *Acta Crystallogr. A* **47,** 110–119.
35. Nakagawa, N., Masui, R., Kato, R. & Kuramitsu, S. (1997) *J. Biol. Chem.* **272,** 22703–22713.
36. Yao, N., Hesson, T., Cable, M., Hong, Z., Kwong, A. D., Le, H. V. & Weber, P. C. (1997) *Nat. Struct. Biol.* **4,** 463–467.
37. Subramanya, H. S., Bird, L. E., Brannigan, J. A. & Wigley, D. B. (1996) *Nature (London)* **384,** 379–383.
38. Korolev, S., Hsieh, J., Gauss, G. H., Lohman, T. M. & Waksman, G. (1997) *Cell* **90,** 635–647.
39. Gorbalenya, A. E. & Koonin, E. V. (1993) *Curr. Opin. Struct. Biol.* **3,** 419–429.
40. Kovalsky, O. I. & Grossman, L. (1998) *J. Biol. Chem.* **273,** 21009–21014.
41. Kovalsky, O. I., Lin, C. G. & Grossman, L. (1998) *Biochim. Biophys. Acta* **1397,** 91–101.
42. Hiratsuka, T. (1982) *Biochim. Biophys. Acta* **719,** 509–517.
43. Lohman, T. M. & Bjornson, K. P. (1996) *Annu. Rev. Biochem.* **65,** 169–214.
44. Marians, K. J. (1997) *Structure (London)* **5,** 1129–1134.
45. Bird, L. E., Subramanya, H. S. & Wigley, D. B. (1998) *Curr. Opin. Struct. Biol.* **8,** 14–18.
46. Lin, J. J., Phillips, A. M., Hearst, J. E. & Sancar, A. (1992) *J. Biol. Chem.* **267,** 17693–17700.
47. Ahn, B. & Grossman, L. (1996) *J. Biol. Chem.* **271,** 21462–21470.
48. Grossman, L. & Thiagalingam, S. (1993) *J. Biol. Chem.* **268,** 16871–16874.

49. Moolenaar, G. F., Visse, R., Ortiz-Buysse, M., Goosen, N. & van de Putte, P. (1994) *J. Mol. Biol.* **240,** 294–307.
50. Kim, J. L., Morgenstern, K. A., Griffith, J. P., Dwyer, M. D., Thomson, J. A., Murcko, M. A., Lin, C. & Caron, P. R. (1998) *Structure (London)* **6,** 89–100.
51. Velankar, S. S., Soultanas, P., Dillingham, M. S., Subramanya, H. S. & Wigley, D. B. (1999) *Cell* **97,** 75–84.
52. Van Houten, B. (1990) *Microbiol. Rev.* **54,** 18–51.
53. Esnouf, R. M. (1999) *Acta Crystallogr. D* **55,** 938–940.
54. Nicholls, A., Sharp, K. A. & Honig, B. (1991) *Proteins* **11,** 281–296.